FUDMA Journal of Sciences (FJS)
ISSN online: 2616-1370
ISSN print: 2645 - 2944
Vol. 7 No. 5, October, 2023, pp 328 - 347
DOI: https://doi.org/10.33003/fjs-2023-0705-1978

INTEGRATING REMOTE SENSING DATA WITH HYDROTHERMAL ALTERATION MAPPING AND GEOCHEMICAL CHARACTERISTICS OF PRECAMBRIAN ROCKS ACROSS MAMBILLA PLATEAU, NORTHEASTERN, NIGERIA

[1]Yohanna Andarawus, [2]Othniel Kamfani Likkason, [3]Maigari Abubakar Sadiq, [2]Ali Sani, [1]Iyakwari Shekwonyadu, *[4]Adamu Abubakar, [1]Frankie Ojo Balogun, [1]Nengak Musa, [1]Ahmad Aliyu Ibrahim

[1]Department of Geology, Federal University of Lafia, Nigeria
[2]Department of Physics, Abubakar Tafawa Balewa University, Bauchi, Nigeria
[3]Department of Applied Geology, Abubakar Tafawa Balewa University Bauchi, Nigeria
[4]Department of Applied Geophysics, Federal University Birnin Kebbi, Nigeria

*Corresponding authors' email: adamu.abubakar35@fubk.edu.ng

ABSTRACT

Mineral exploration must include the mapping of hydrothermally altered regions, which are typically connected to mineralization. This study presents a strategy for integrating remote sensing data with the geochemical characteristics of Precambrian rocks from the Mambilla Plateau in northern Nigeria. Tectonically, the lineaments were fractures with the following orientations: NE-SW, NW-SE, ENE-WSW, and N-S. The distinct spectral reflectance and absorption properties of remotely sensed Landsat 8 data in the visible, near-infrared, shortwave-infrared, and thermal infrared portions of the electromagnetic spectrum were exploited in various digital image processing approaches. Mapping hydrothermal alteration minerals was done effectively and efficiently using band ratios (red/blue, SWIR 2/NIR, SWIR 1/NIR), spectral band combinations (Kaufmann and Sabins ratios), and principal component analysis. Ferric, phyllic, propylitic, and argillic iron all underwent changes as a result of hydrothermal alteration. Regional metamorphism also resulted in important alteration processes such as epidotization, sericitization, muscovititization, kaolinitization, and chloritization. Geochemically, on average, the Al_2O_3, SiO_2, Fe_2O_3, CaO, MgO, K_2O, Na_2O, Li_2O content are 12.04 %; 54.83%; 4.76%, 7.16%, 3.02%, 10.22%, 4.53%, 1.35% while MnO, P_2O_5 and TiO_2 are less than 1%. The average base metal composition revealed that 60% of them had positive anomalies, which indicate mineralization, and 40% had negative anomalies. About 50% of the samples had positive anomalies, which indicated strong potential for harbouring mineralization based on the makeup of trace elements. Geochemical studies revealed the presence of lithium, titanium, and silica oxides in substantial concentrations. The local mineralization is governed by structural factors.

Keywords: Remote sensing datasets, Hydrothermal alteration mapping, Geochemical characteristics, Mineralization potentials, Precambrian rocks

INTRODUCTION

Mineral exploitation and exploration are crucial for the economic development of many emerging nations. In general, traditional mineral exploration techniques are expensive, time-consuming, and labour-intensive, especially in remote areas. Mineral exploration requires geological, geochemical, and geophysical datasets, but they may not always be available or may not exist in places that are difficult to access (Kaiser et al., 2002; Bemis et al., 2014; Maduaka, 2014). Exploration of minerals also involves state-of-the-art techniques and expertise. Modern remote sensing technology has proven to be one of the most efficient and trustworthy approaches for mineral exploration. When using remote sensing satellite images for geological mapping and mineral exploration, it is usually necessary to study the physicochemical properties of rocks and weathering soils, including mineralogy, landforms, geochemical signs, and the spatial distribution of lineaments (Bhattacharya et al., 2012).

The idea that undiscovered minerals could exist alongside discovered ones is a cornerstone of the mineral exploration field. For example, similar minerals will probably be found closer to the discovered deposit if mining is planned there, and the likelihood of finding new deposits will decrease with increasing distance. When that occurs, remote sensing—mostly through multi- or hyperspectral remote sensing images—can be effectively used to identify areas with higher odds of mineralization before drilling exploratory boreholes at new locations (Gholamie et al., 2012; Ciampalinie et al., 2013). Reflectance spectroscopic data generated from remote sensing data reduces the time and cost of fieldwork needed for geological, geophysical, and geochemical studies (Short and Lowman Jr., 1973; Tedesco, 2012; Marjoribanks, 2010). Numerous remote sensing studies for lithological mapping and mineral prospecting have been carried out in arid and semi-arid environments. In areas with favourable geological exposure, satellites in orbit can directly gather data on spectral reflectance from rocks or soils (Sabins, 1999; DiTommaso and Rubinstein, 2007; Zhang et al., 2007; Pour and Hashim, 2012; Mahboob et al., 2015).

As a tool for the early stages of porphyry copper and epithermal gold exploration, multispectral and hyperspectral remote sensing data can be used to identify hydrothermal alteration minerals with diagnostic spectral absorption properties in the visible, near-infrared, and shortwave length infrared regions (Di Tommaso and Rubinstein, 2007; Zhang, Pazner, and Duke, 2007; Ramakrishnan and Bharti, 2015). Fluids are often modified hydrothermally to produce porphyry copper deposits. Pour and Hashim (2012) claim that these altered rocks can be recognised by their visible and infrared spectral characteristics. With a certain amount of electromagnetic (EM) radiation reflected and/or absorbed at a specific wavelength, many minerals have unique and recognisable spectral characteristics that can be used to confidently identify them. This part of the electromagnetic spectrum (between 0.4 and 2.5 m; visible, near-infrared, and shortwave-infrared) is where most sunlight is reflected, so it can be used to identify geological features that have low- and moderate-temperature characteristics (Mahboob et al., 2015a). In this region of the electromagnetic spectrum, iron oxides, oxyhydroxides, and ligands can usually be mapped very well because of their properties that alter at high or low temperatures (Clark et al., 1990). This part of the spectrum can also be used to differentiate between silicate (clay) minerals and other characteristics. The spectral differentiation of minerals has been the driving force behind the application of this technology in mineral discovery (Calvin et al., 2015). The wavelength of the thermal infrared (TIR) component of the spectrum, which usually spans from 7 to 14 m, is used to detect the energy emitted from Earth's surface. In addition to water, carbonates, and sulphates, this part of the electromagnetic spectrum is sensitive to Si-O bonding in silicates (Repacholi, 2012; Udvardiet al., 2017; Manley, 2014). Calcite, orthoclase feldspar, kaolinite, montmorillonite, and haematite are among the common minerals whose spectral characteristics can be reliably and clearly mapped using reflectance spectroscopy data. The underlying or surface evidence of these deformation events is rarely found or mapped. But this problem presents an opportunity for our research, so we use an integrated approach of remote sensing datasets with hydrothermal alteration mapping and geochemical features of the metals in the rear Earth to propose solutions to the problems mentioned above.

The geochemical characteristics were utilised to identify the primary alteration processes responsible for the mineralization potentials found in the Pre-Cambrian rocks of the Mambilla plateau in northeastern Nigeria, as well as to calculate the crustal abundance of base metals. The tectonic history, surface lithology, lineament mapping, and structural mapping of the study area were all conducted using the remote sensing datasets.

Study area Location and its Geological settings

The study area is located in northeastern Nigeria, in the Taraba State parts of Sardauna and Gashaka. With a total landmass of around 6160 km^2, its boundaries are determined by the longitudes 6° 30' 00" E and 7°30' 00"E and the latitudes 11° 00' 00" N and 11°30' 00"N (Fig. 1). The Mambilla plateau forms the southernmost tip of the eastern part of northern Nigeria in the sub-Saharan Sudan area of West Africa (Frantz, 1981; Tukur*et al.*, 2005). The area has an average annual rainfall of roughly 30 inches, and the wet season spans from April through October. The environment and vegetation are reminiscent of a Savannah. The long dry season, which spans from November to March, is characterised by dusty harmattan breezes from the northeast. With occasional highs of 105 °F, April and May are the hottest months. The Basement Complex rocks, which span from the Precambrian to the early Paleozoic, overlay the plateau. The plateau and its environs are also composed of volcanic rocks that date from the upper Cenozoic to the Tertiary and Quaternary ages (Jeje, 1983; Mubi and Tukur, 2005). These rocks were extruded from tectonic fault lines within the plateau and are volcanic in origin. This volcanic rock is composed of olivine basalt, basalt suite, and trachyte basalt, all of which contain various combinations of amphiboles, pyroxenes, and other free quartz minerals (Mould, 1960). Tertiary basalts, primarily formed by trachytic lavas and widespread basalts, are found on the Mambilla Plateau (Dupreez and Barber, 1995). These crystalline basement rocks underwent progressive deformation of varying intensities over time, resulting in the formation of major fractures. Consequently, N to S, NE to SW, NW to SE, NNE to SSW, NNW to SSE, and, to a lesser extent, E to W are the trends of the fractured (Obaje, 2009).

The Basement Complex (Fig. 2) is one of the three primary litho-petrological components that comprise Nigeria's geology. The Nigerian Basement Complex is part of the Pan-African mobile belt; it is situated between the West African and Congo Cratons, south of the Tuareg Shield. The Cretaceous and more recent sediments are unevenly layered on top of the Mesozoic calc-alkaline ring complexes, or newer granites, that penetrate the Jos Plateau. The Nigerian basement was influenced by the 600 Ma Pan-African orogeny. It is situated in the reactivated zone formed by plate collisions between the active Pharusian continental margin and the passive continental margin of the West African craton (Burke and Dewey, 1972; Dada, 2006). The deformation, metamorphism, and remobilization of the basement rocks are believed to have been greatly influenced by the Liberian (2,700 Ma), Eburnean (2,000 Ma), Kibaran (1,100 Ma), and Pan-African (600 Ma) cycles. Among the ore minerals found in the Oban-Obudu-Mandara-Gwoza region in the eastern part of the Nigerian Basement Complex are gem minerals and cassiterite, wolframite, galena, chalcopyrite, and barite (Obaje, 2009).

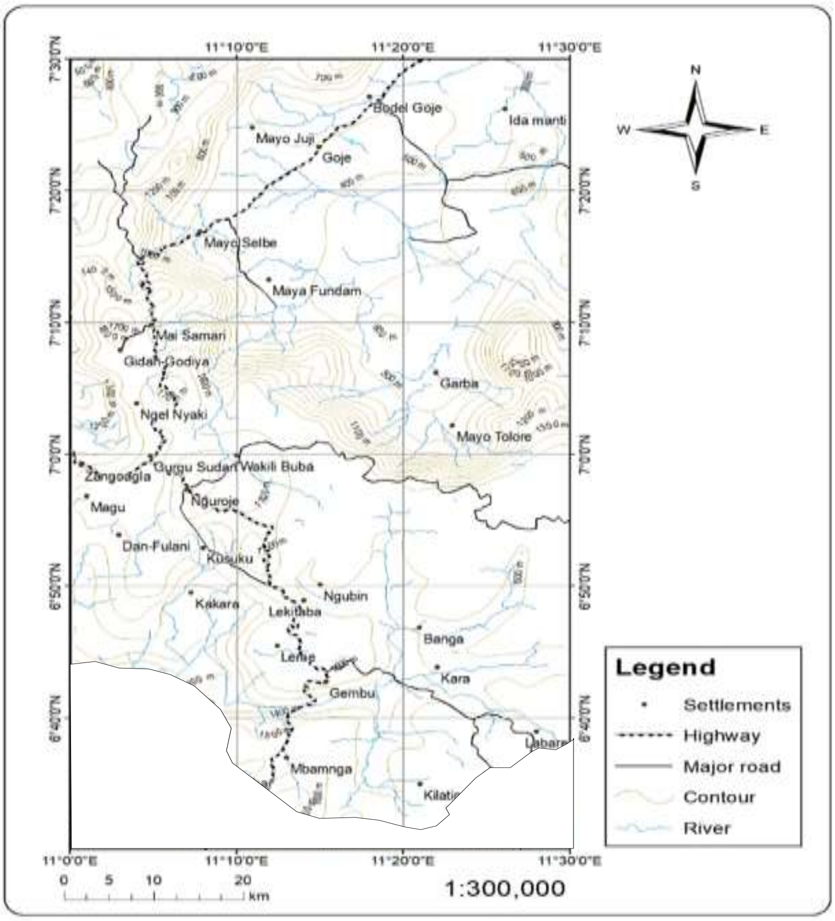

Figure 1: Map showing the location of the Study area (Adopted from Arch-GIS, 2019)

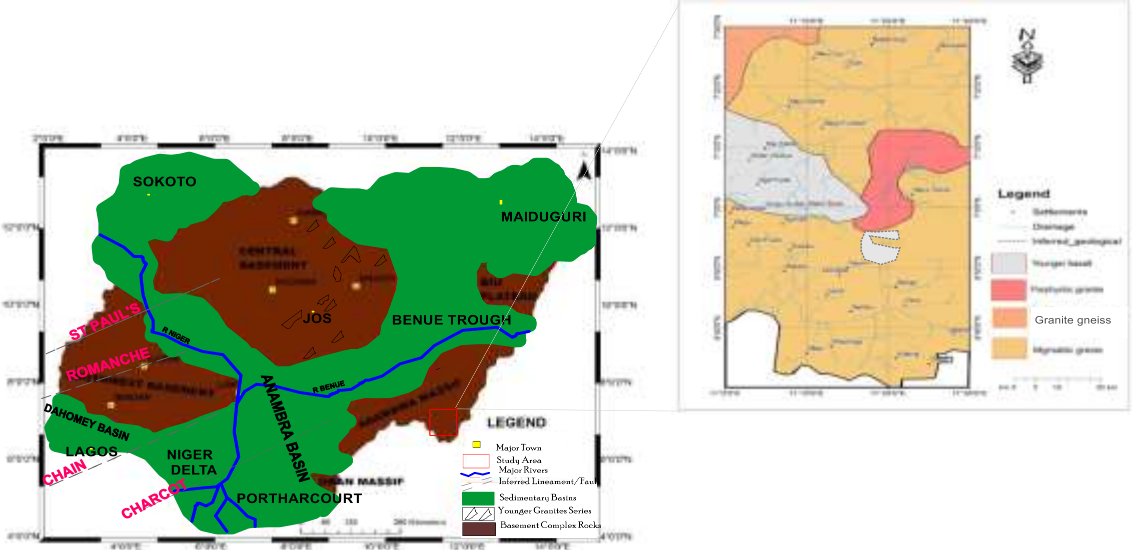

Figure 2: The Geological map of the Study area, Showing the rock types, and their lithologies (Modified after Dada, 2006; Obaje, 2009)

MATERIALS AND METHODS

Digital Elevation Model

As an endless spatial representation of the ground's topography or elevation, digital elevation models (DEMs) are easiest to define (Abrams et al., 2020). Their application to geology is very valuable in understanding the local structural architecture of rocks and areas (Fig. 3). In order to obtain the ASTER DEM, which was launched in 1999 and used for lineament generation in this study, the United States Geological Survey Agency Earth Resource Observation and Science (USGS-EROS) website was consulted (accessed on August 29, 2021). The elevation data for the latitudes 83^{o}N and 83^{o}S in the ASTER DEM, which is freely accessible from NASA and Japan's MITI, has a tile size of 1^{o} x 1^{o} and a spatial resolution of 30 m. To create these data, 1.3 million Level 1A scene photos that were taken between March 1, 2000, and November 30, 2013, were combined. Stacking all of the individual cloud masks and non-cloud mask scenes was the first step in creating a DEM. The appropriate algorithm was subsequently used to apply unwanted data. A DEM was used in this work to extract lineament data from the study area. DEM was chosen because of its high resolution and ability to extract lineaments with a geological origin (Dos Santos et al., 2016).

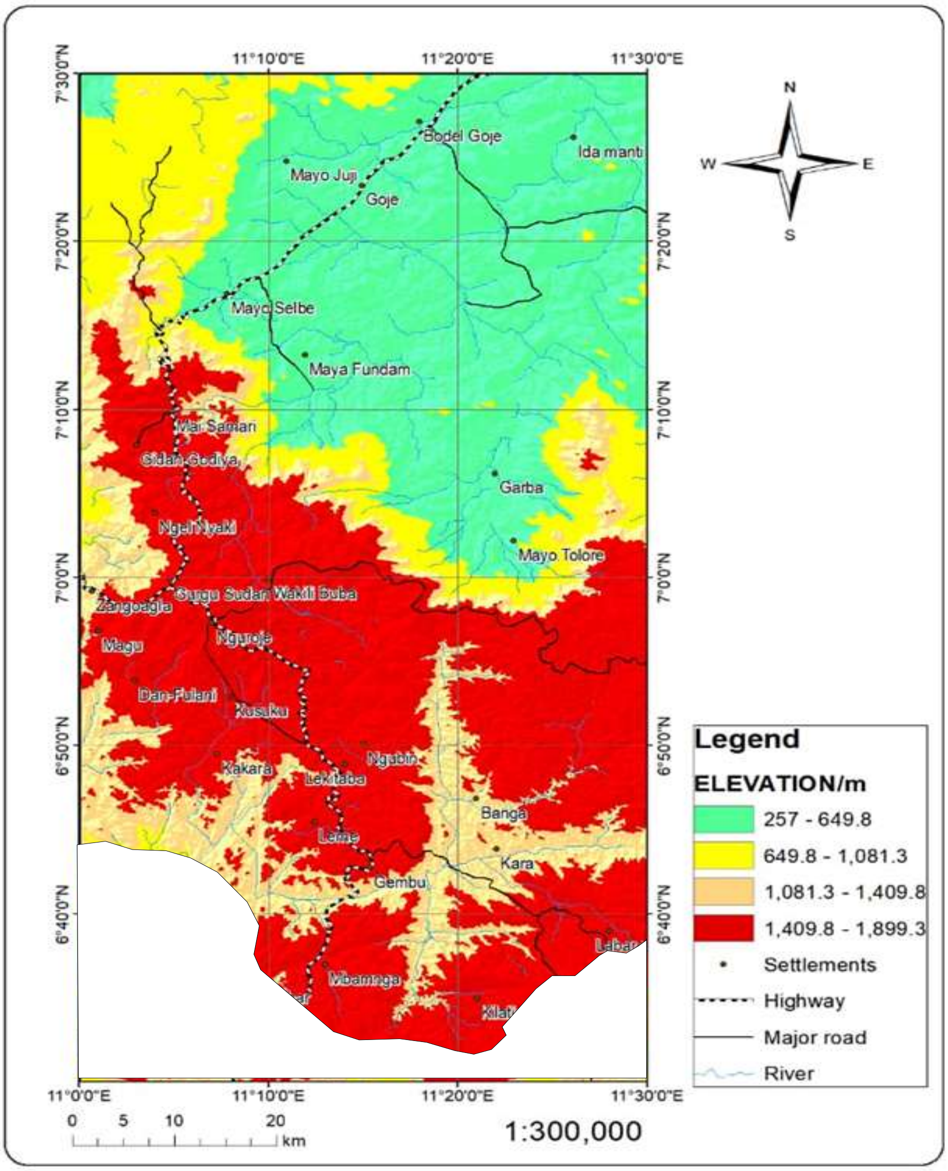

Figure 3: Map of digital elevation model (DEM) of the study area, showing low elevations within the northern parts and surrounded by high elevations (south to west regions) indicative of exposed basement.

Remote Sensing data

The most often used satellite data for mapping and investigating hydrothermal minerals is usually ASTER. However, due to malfunctions, six of ASTER's SWIR sensors have not been used since 2008 (Wesselset et al., 2013). Free Landsat data is used for research and mapping of hydrothermally altered minerals and rocks. This study used cloud-free level 1T (L1T) information collected in August 2017 (path 170/row 78) of the Landsat 8 satellite. Absolute radiance units are computed using 32-bit floating-point estimations during the processing of Landsat images. These data are transformed into 16-bit integer values in the final Level 1 product (Chander and Markham, 2003). Table 1 lists the spectrum and geographic properties of the functional Landsat 8 Thermal Infrared Sensor (TIRS) and Land Imager (OLI). A region measuring 170 km by 183 km (north to south) is covered by a single Landsat 8 image.

Satellite image pre-processing

Pre-processing is required in order to create geometrically and atmospherically corrected satellite images, which are then used to extract and analyse the spectral data. The method known as geometric correction involves the use of georeferencing satellite images with respect to terrestrial control points for the purpose of generating pixels of the same size. There are two other approaches to atmospheric corrections: total correction (Chavez, 1996; Song and Woodcock, 2003) and comparison normalisation (Schroeder et al., 2006). Relative normalisation, according to Song et al. (2001), is the process of radiometrically adjusting the Landsat data sets with respect to a reference image using the Pearson correlation between objects that are pseudo-invariant through various dates. Empirical and physical-based approaches are two further categories into which absolute correction can be separated. The empirical method converts the spectrum data from the sensor's luminescence to ground reflectance using the spectral characteristics of the ground attributes. While empirical approaches are simple to use, they do not take into consideration the variation in atmospheric influence from pixel to pixel. On the other hand, the heterogene is accounted for by physical-based techniques like the Satellite Signal in the Solar Spectrum (6S) code (Vermoteet al., 1997), MODERATE-resolution atmospheric TRANsmission (MODTRAN) (Berket al., 1998), and Atmospheric/Topographic Correction (ATCOR) (Richter, 1997). However, because the Landsat Ecosystem Disturbance Adaptive Processing System (LEDAPS) software (Maseket et al., 2006) implemented the 6S code, atmospheric correction for Landsats 4–7 was fully automated. Vermote et al. (2016) have developed an enhanced atmospheric correction algorithm for Landsat 8 (L8SR) that shows promise over the haphazard Landsat 5-7 LEDAPS product (Table 1).

Table 1: Landsat 8 satellite spectral and spatial detail

Spectral band number	Spectral band name	Wave length(μm)	Spatial resolution(m)
1	Coastal aerosol	0.43 - 0.45	30
2	Blue	0.45 - 0.51	30
3	Green	0.53 - 0.59	30
4	Red	0.64 - 0.67	30
5	Near-Infrared (NIR)	0.85 - 0.88	30
6	Shortwave-Infrared (SWIR) 1	1.57 - 1.65	30
7	Shortwave-Infrared (SWIR) 2	2.11 - 2.29	30
8	Panchromatic	0.50 - 0.68	15
9	Cirrus	1.36 - 1.38	30
10	Thermal-Infrared (TIRS) 1	10.60 - 11.19	100
11	Thermal-Infrared (TIRS) 2	11.50 - 12.51	100

Spectral sub setting

Since OLI band 1 (coastal aerosol) is useful for imaging shallow waters and band 9 (cirrus) is useful for spotting high-altitude clouds and monitoring small particles like dust and smoke, these two bands were excluded from the analysis afterwards. Moreover, research indicates that the best bands for mineral exploration mapping are found in the visible, near-infrared, and shortwave ranges. In this investigation, OLI bands 2–7 and TIRS bands 10–11 were utilised for additional processing. All of these bands were merged into a single image using the layer stacking digital image processing technique (Mahboob et al., 2015).

Digital number conversion to reflectance

The Landsat 8 L1T pictures often contain digital quantities (DNs), which must be translated to surface reflectance because they lack any physically significant information. Since it takes into account the solar circumstances (lighting, intensity, and geometry) at the time the photos were taken, this conversion is necessary for quantifying various attributes in remote sensing data. The data in this study were converted to top-of-atmosphere (TOA) reflectance using radiometric coefficients, as recommended by Roy et al. (2016). After that, DNs were transformed into reflectance, as seen in Figure 4, which is the ratio of radiation striking a surface to radiation reflected from it (Han and Nelson, 2015). DN data were transformed to TOA reflectance using Equation (1) (Zanter, 2016):

$$\rho\lambda = \frac{M_{\rho} \times Q_{\text{cal}} + A_{\rho}}{\sin\theta} \qquad (1)$$

Where θ = Solar elevation angle (degrees), Q_{cal} = Level 1 pixel value in DN, $A\rho$ = Reflectance additive scaling factor for the band, $M\rho$ = Reflectance multiplicative scaling factor for the band, and ρ_{λ} = Top of Atmosphere Planetary Reflectance (dimensionless).

Reflectance spectroscopy of satellite imagery

Based on the spectral absorption characteristics, the data gathered by Landsat 8 can be used to identify various components and surface features. It shows the reflected and/or emitted spectrum energy. The EM spectrum absorption properties of certain minerals and mineral groups in hydrothermally altered rocks are unique. Several alunite and clay ores, for example, exhibit characteristic absorption at approximately 2.1 m, and their spectral responses are significantly stronger at approximately 1.7 m (Sabins, 1999). Iron oxide and sulphate, according to Johnson et al. (2016), usually show low and high reflectances in the ultraviolet/blue and near-infrared regions of the electromagnetic spectrum, respectively. Consequently, in an image with natural colours, these minerals seem rusty.

Band rationing of satellite imagery

Band-ratioing is a digital image-processing technique that enhances the contrast between features by dividing the reflectance for the pixels in one band of the same satellite image by the reflectance for the pixels in another band. This technique has been widely used to map and visualise rocks that have experienced hydrothermal alteration. For example, Han and Nelson (2015) used Landsat Thematic Mapper (TM) band 5 (1.55–1.75 m) image ratios over band 7 (2.09–2.35 m) to successfully distinguish between areas with significant concentrations of alunite and clay, where pixels in the satellite image appear bright. In a different study, Van der Meer (2004) used the ratio image of band 3 (0.63-0.69 m) over band 1 (0.45–0.515 m) to pinpoint areas that are rich in iron ores. For enhanced lithological units and rocks that had undergone hydrothermal alteration, various band ratios were developed in the current research work, as indicated in Table 2. The bands selected are determined by the location of the absorption bands and the spectral reflectance of the mineral or mineral assemblage under mapping. The band-ratioing method is a great way to visualise data, but it is not able to map or measure the area's characteristics. Part of the reason for this limitation is that most optical multispectral remote sensing devices have bandwidths > 0.05 m, which are too big to effectively discriminate between the numerous spectral absorptions connected to different alteration minerals (van derMeer, 2004). Furthermore, many band ratio methods only employ two or three bands, but multispectral remote sensing instruments provide far more bands than those mentioned above. Due to these limitations, a more sophisticated digital satellite image analysis technique that is capable of simultaneously utilising all of the satellite bands must be used.

Table 2:Band ratio of enhancement of hydrothermally altered rocks

S/N	Spectral band name	Wave length(nm)	Type of mineral enhanced
1	$\frac{\text{red}}{\text{blue}}$	640–670 450–510	Iron oxide
2	$\frac{\text{Shortwave} - \text{Infrared (SWIR) 1}}{\text{Shortwave} - \text{Infrared (SWIR) 2}}$	1570–1650 2110–2290	Hydroxyl- bearing rock
3	$\frac{\text{Shortwave} - \text{Infrared (SWIR) 2}}{\text{Near} - \text{Infrared (NIR)}}$	2110–2290 850–880	Clay minerals
4	$\frac{\text{Shortwave} - \text{Infrared (SWIR) 1}}{\text{Near} - \text{Infrared (NIR)}}$	1570–1650 850–880	Ferrous mineral

Spectral band combination

The spectral band combination approach, also known as red-green-blue (RGB) combination, is a very useful image-enhancement technique that offers powerful ways to visually comprehend multispectral satellite data (Novak and Soulakellis, 2000). Satellite data band combinations can be real (natural) or false-colour composites (FCC) based on particular bands or band ratios. Over time, a variety of band ratios and band combinations have been developed to help distinguish lithologies in satellite images (Table 3). The hydrothermally altered rocks were mapped using the Kaufmann and Sabins ratios in relation to the local minerals. These two ratios have been applied to determine altered places and the minerals contained within a rock. The Kaufmann ratio was used by Mia and Fujimitsu (2012) and Abhary and Hassani (2016) to map minerals that contained iron and hydroxyl ions. In order to identify sulphide deposits associated with iron oxide alteration zones, Da Cunha Frutuoso (2015) used the Sabins ratio. This technique was used in this study.

(a)Principal Component analysis

Principal component analysis (PCA) yields proficient information that is regularly used in the earth sciences (Cheng et al., 2011; El-Makky, 2011). PCA is a widely used multivariate statistical method that is commonly employed to examine correlations between variables. Many correlated variables can be orthogonally transformed into uncorrelated combinations (eigenvector loadings) of principal components (PCs) based on their covariance or correlation matrix (Horel, 1984; Loughlin, 1991). The highest degree of variability in the original data set is usually not highlighted by many PCs (Panahi et al., 2004). Because PCA reduces the dimensionality and redundancy of data sets, it is therefore widely used to improve the interpretability of information (Cheng et al., 2011; Horel, 1984; Jolliffe, 2002). According to the PCA algorithm, which states that PCs are linear combinations of the original variables, PCs integrate the input variable uniquely and indicate only a small amount of information within the entire dataset (Abdi and Williams, 2010). Because PCA can handle multivariate data sets, it has been extensively used in remote sensing for geological mapping of ores and igneous rock strata (Grunsky et al., 2014). The spectral characteristics of different features in the area, like plants, rocks, and soils, usually cause the statistical variance mapped onto each PC, which is the foundation of the Crosta technique (Tangestani and Moore, 2001). This work has applied the method based on highly fluctuating non-correlated satellite bands for hydrothermally altered rocks.

Table 3:Landsat TM spectral band combinations, RGB combinations for enhancement of hydrothermally altered rocks

S/N	Analysis type	Spectral bands	Type of mineral enhanced	References
1	Kaufmann ratio	$\frac{7}{4}:\frac{4}{3}:\frac{5}{7}$	Iron-ion-containing minerals are represented by red, vegetated areas by green, and hydroxyl-bearing minerals by blue.	(Kaufmann, 1988)
2	Chica–Olma ratio	$\frac{5}{7}:\frac{5}{4}:\frac{3}{1}$	Color-wise, red stands for clay, green ferrous ions, and blue for ferric ions.	(Mia and Fujimitsu, 2012b)
3	Sabins ratio	$\frac{5}{7}:\frac{3}{1}:\frac{3}{5}$	Areas of hydrothermal alteration are shown by yellow; water is indicated by black; vegetation is shown by dark green, rocks rich in clay by lighter green; sand is shown by blue; and iron oxides are indicated by red, pink, or magenta.	(Sabins, 2007)
4	Sultan's ratio	$\frac{5}{7}:\frac{5}{1}:\frac{5}{4}\times\frac{3}{4}$	The hydroxyl minerals are represented by deep violet, ferric ions by green, and ferrous oxides by blue.	(Gad and Kusky, 2006)
5	Abrams ratio	$\frac{5}{7}:\frac{3}{1}:\frac{4}{5}$	Clay minerals are red, and hydrothermally changed iron oxide is green..	(Pour and Hashim, 2012)

(b)Lineament Extraction Analysis

Since geological structures are essential to the formation of mineral deposits, they were mapped using a variety of spatial data on a regional scale (Tripp & Vearncombe, 2004). Previous research (Sadiq et al., 2022; Abdul Malik et al., 2018) indicates that manual, automatic, or semi-automated methods have been used to extract geological lineaments. However, for this study, lineaments were automatically extracted. Automated methods have received recognition for their efficacy and reproducibility (Weerasekara et al., 2014). Specific software settings (Table 4) on PCI Geomatica v10.0 aided in the spatial extraction of lineaments from DEM (Figure 1). Lineament extraction was followed by statistical and spatial analyses, such as orientation and lineament density analyses using rose plots (Hung et al., 2005) and dip histograms (Immaculate et al., 2020).

Fieldwork and Laboratory Techniques

The field study included a description of the structural contexts and field relationships of the exposed rock units in the area. Ten distinct rock samples (Table 5) were collected in total. On ten selected samples, comprehensive megascopic analyses were performed. Major and uncommon base metals were analysed in each sample using a Philips X-ray fluorescence (XRF) spectrometer (PW/2404) equipped with a Rh radiation tube and eight analysing crystals (EMRA).

Table 5: Description of rock samples and their coordinates in the study area

S/No.	Samples Type	Latitudes (N)	Longitudes (E)	Elevation (m)	Rocks Type/Remarks
1	S01	11°21′30.9″	7°29′54.4″	363	Vein
2	S02	11°21′ 30.9″	7°24′34.4″	365	Vein
3	S03	11°21′ 30.9″	7°21′05.6″	418	Vein
4	S04	11°21′ 30.9″	7°19′00″	518	Quartz vein
5	S05	11°21′ 30.9″	7°15′31.3″	622	Vein
6	S06	11°21′ 30.9″	7°12′31.2″	1543	Vein
7	S07	11°21′ 30.9″	7°14′22.7″	1501	Vein
8	S08	11°21′ 30.9″	7° 7′53.5″	1469	Vein 6 inches thick.
9	S09	11°21′ 30.9″	7°7′38.4″	1790	Vein
10	S10	11°21′ 30.9″	7° 04′51.1″	1603	Vein

RESULTS AND DISCUSSION

Lithological mapping in the Study Area

(a) Principal Component analysis (PCA)

In order to characterise the lithologies, the colour composition (CP3, CP6, CP1) RGB created from eight Landsat OLI bands was utilised. The results correspond with the geological map of Figure 2 and include the following lithologies: younger basalt, porphyritic granite, granite gneisses, and migmatite gneisses (Fig. 4). This technique is widely applied in remote sensing to compress the data dispersed across our Landsat 8 OLI image's multiple spectral bands. The new components of this technique often represent up to 97% of the original dataset (Deslandes, 1989).

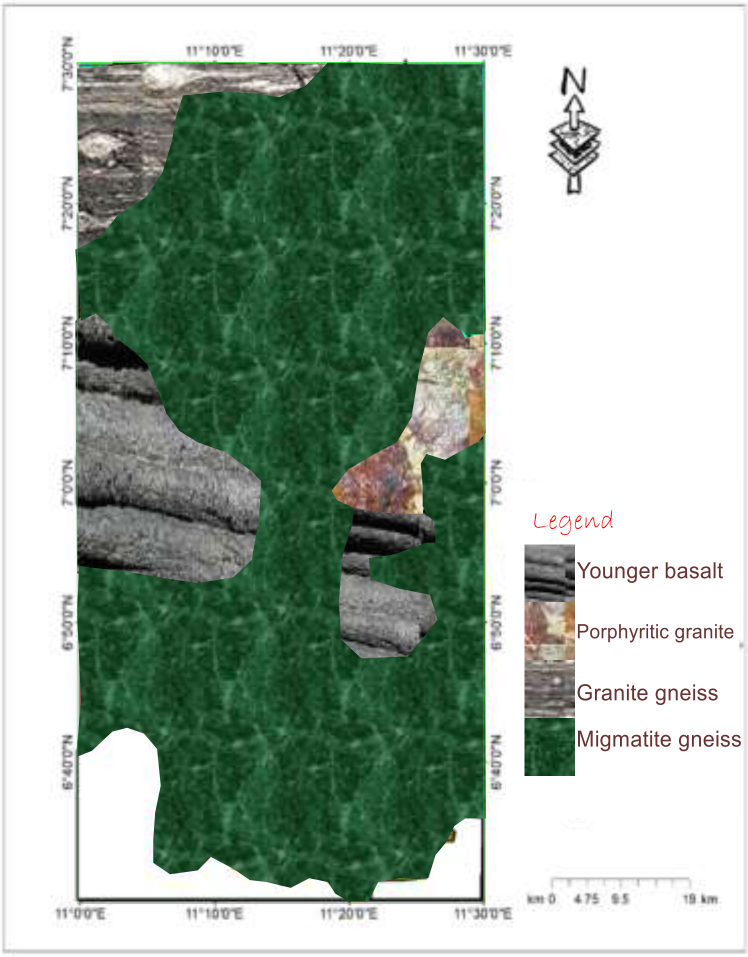

Figure 4: Color composite of the Landsat OLI image, using (CP_3, CP_6, and CP1, in RGB) showing younger basalt (yb), porphyritic granite (pg), granite gneisses (Gn) and migmatite gneiss (Mg).

(b) Band ratios (BR) and Supervised Classification approach

Three band ratios (7/6, 6/5, 4/2; 7/2, 4/2, 6/7); and (6/4, 6/2, 7/6) were effectively employed in the current study. Figure 5 shows the lithologies that were identified: migmatite gneiss, porphyritic granite, younger basalt, and granite gneisses. According to Kruse, Fred et al. (1993), the result corresponds with the geological map in Figure 2. The results show that these band ratios are highly helpful in distinguishing between the different rock types in the study area. Its basis is a physical principle called prototype spectra, also referred to as "end members," which determines the degree of similarity between each picture pixel's spectrum and the reference spectra. A spectroradiometer can be used to directly measure both of these in the field based on an image (Plaza and Chang, 2005; Kruse et al., 1993; Richards, 1999). It considers all of the image's spectral bands in a "N-dimensional" spectral space and requires radiometrically and atmospherically calibrated and standardised image data (Boardman and Kruse 1994). The basic goal of band ratios is to enhance the spectral dissimilarities between lithological units. New colour compositions can now be added to the band ratio calculations.

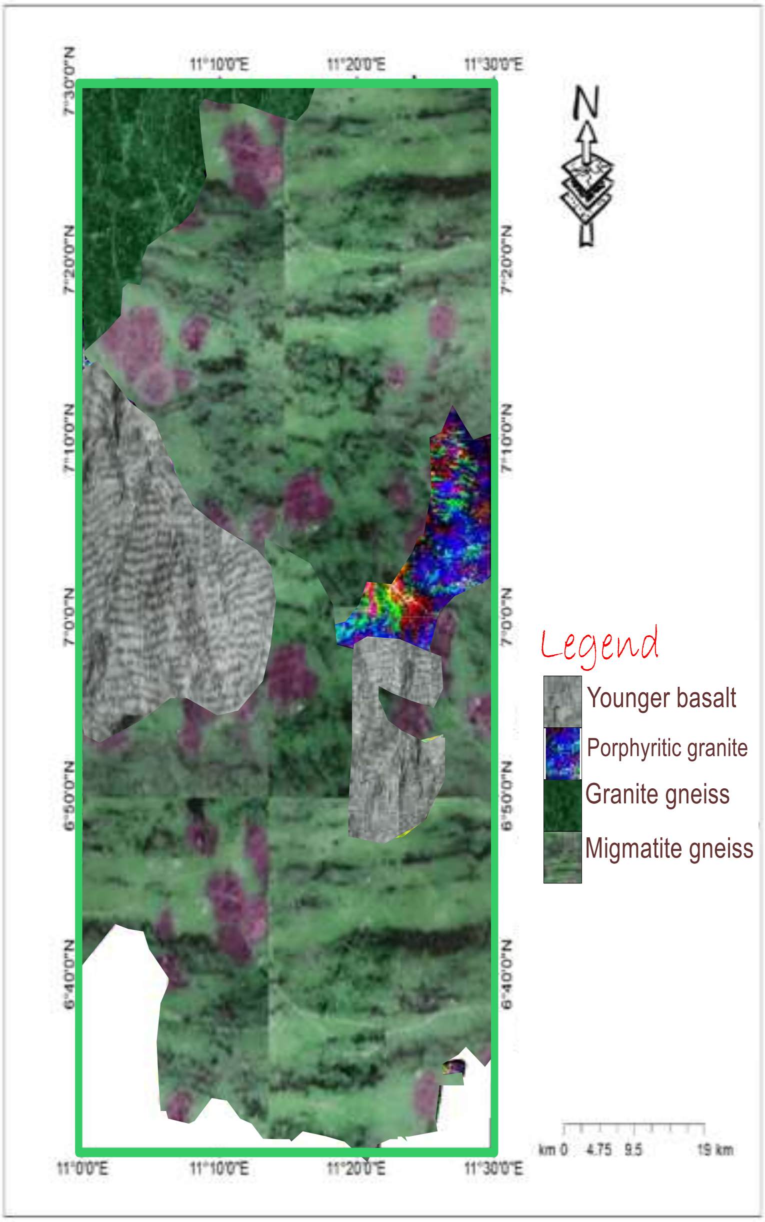

Figure 5: The RGB colored compound of the divisions (ratio) of bands: [(7/6); (6/5); (4/2)] showing Younger basalt (Yb), porphyritic granite (Pg), granite gneisses (Gn) and migmatite gneisses (Mg)

Hydrothermal alteration mapping

Remote sensing for the identification and mapping of hydrothermal minerals is only beneficial if it is possible to discriminate clearly between the reflected spectra of altered bedrock and those of other objects. The true colour composite of bands 2, 3, and 1, which were red, green, and blue, respectively, emphasised the textural characteristics of the rocks, which set them apart from other rocks. Pournamdari et al. (2014) tested the same combinations of satellite bands and found that they could be used to distinguish between igneous and non-igneous rocks. The false-colour composite was assigned to bands 4, 3, and 2 as red, green, and blue, respectively, in order to analyse the reflected satellite spectroscopic data (Fig. 5). The false-colour composite is essential for emphasising the regional geological and geomorphological features, according to Bedini (2009) and other sources. The vegetation appeared to be in red tones due to the presence of the near-infrared (0.7–1.2 m) band, where the vegetation reflects most of the light and is emphasised with a red colour.

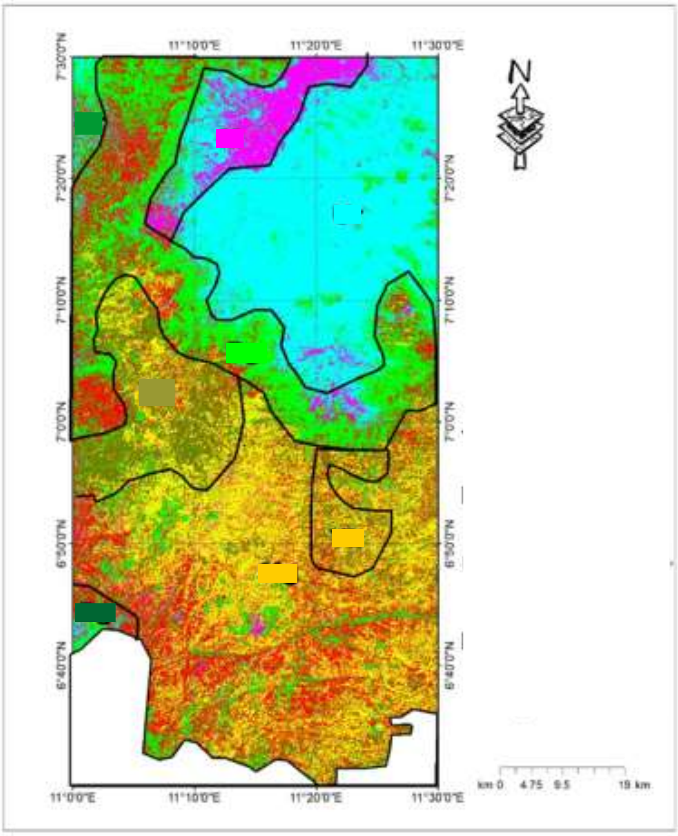

Figure 6: Band ratio for enhancement of potential mineralization in the study area. Red and blue band represent soil with potential for iron mineralization, yellow and purple enhance areas with potential clay minerals and orange to yellow represent areas with potential ferrous oxides.

Hydrothermally altered clay and carbonate minerals can be identified by yellow patches in crystalline igneous rocks (Fig. 6).This could be due to the reflectance of clay and carbonate minerals at 1.55–1.75 m (Landsat 8 band 6) and absorption in the 2.1–2.4 m range. Van der Meer (2004) also reported the same absorption and reflectance bands for the clay minerals using data from NASA's Airborne Visible/Infrared Imaging Spectrometer (AVIRIS). Another study by Zainiet al. (2016) found that clay and carbonates share the same absorption and reflectance bands, which were used to map them using reflectance spectroscopy. The investigation conducted by Holmes and Lu (2015) corroborated the results of this study. No remotely detected satellite image can be used to "see" sapphire, quartz, or tourmaline up close. This precious metal's distribution can be mapped by combining it with various other minerals based on their spectral reflectances (Kotnise and Chennabasappa, 2015). Clay minerals such as illite, dioctahedral smectite, and kaolinite are generally found in the alteration zones associated with mineral deposits such as sapphire and tourmaline (Drews-Armitage et al., 1996). Specific electromagnetic spectral signatures, mainly in the shortwave infrared range, are present in these minerals. These spectral fingerprints are a very economical and efficient way for mineral exploration programmes to map the probable locations of sapphire, tourmaline, and lithium deposits. The band combination of short-wave infrared 2, which has a wavelength of 2.11-2.29 m, and near-infrared, which has a wavelength of 0.85-0.88 m, The iron oxides that were present in the study locations were highlighted by the red-to-blue band ratio, as shown in Table 2. Rich soils with iron oxides reflect more light in the red spectrum (0.64-0.67 m) and absorb more light in the blue spectrum (0.45-2.51 m), according to Schwertmann (1993). The typical reflectance of iron oxide-rich soils is shown in Figure 7. The significance of the red and blue bands of Landsat data for mapping iron oxides has also been demonstrated by Pour and Hashim (2015). Using spectral band ratio approaches, Pour and Harshim (2012) also recognised the iron-rich mineralized zones of distant Antarctica in Landsat imagery.

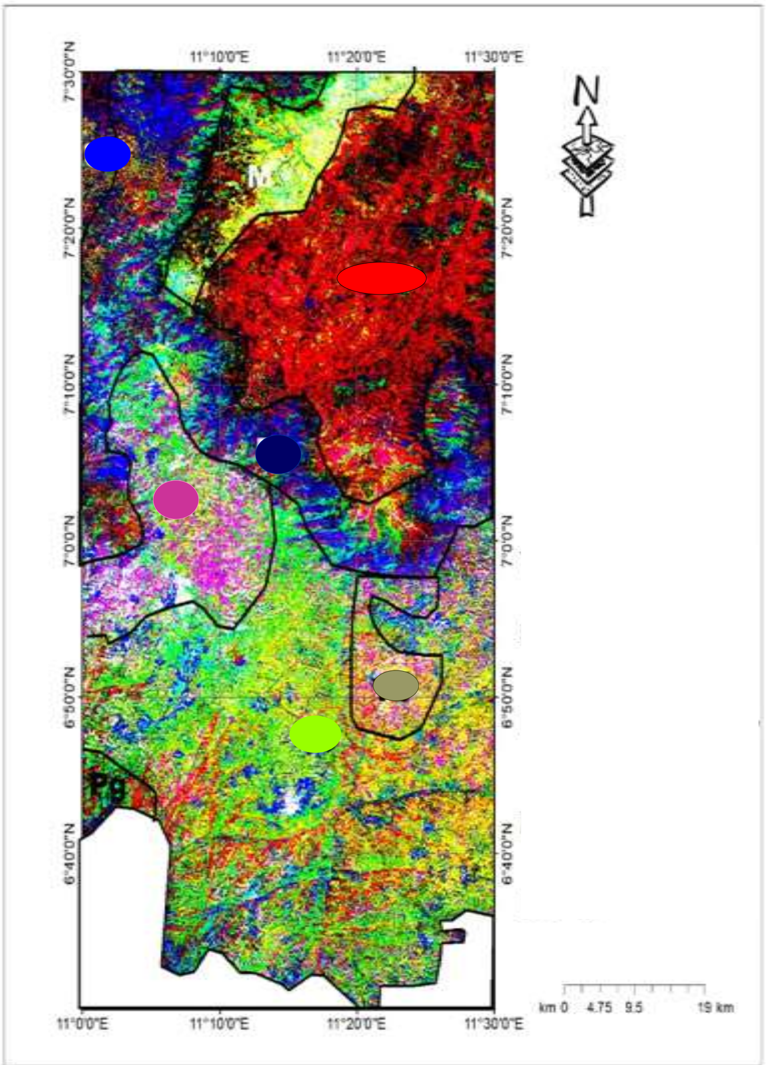

Figure 7: Landsat TM spectral band combinations map of the study area using Kaufmann and Sabins ratio for enhancement of hydrothermally altered rocks. Red represents minerals containing iron; green represents vegetated zones, and blue represent hydroxyl-bearing minerals, and lighter green signifies clay-rich rocks

Application of lineament analysis and its significant to mineralization

Figure 8 displays the main lineament map of the study area. Visual inspection of Figures 8 and 9 indicates that the lineaments in this image appear to be oriented in different directions, but mainly trend in the NE-SW, N-S, NNW-SSE, and NW-SE directions. These dips are most noticeable at 30° to 40° (Figure 10). Diverse lineament patterns within the research area suggest a complex tectonic past, according to Yusuf et al. (2019). Per the results of the lineament density study, the lineaments were concentrated in the centre of the area (at the artisanal mining areas), from which the compression gradually expanded northeastward. This area had a high degree of fracturing and lineament density. Zones of high lineament density (Ananaba and Ajakaiye, 1987) are crucial for the mineral deposits' location (Fig. 11). According to the analysis of rose diagram plots (Figs. 8 and 9) for these lineaments, the NE-SW and NW-SE directions are more common than the N-S and NNW-SSE trends. Ibrahim (2013) regarded the ENE-WSW lineaments as right and left lateral slip faults and the NW-SE lineaments as left-lateral strike slip faults. Additionally, the main dips' histograms (Figure10) show a 30°–40°.

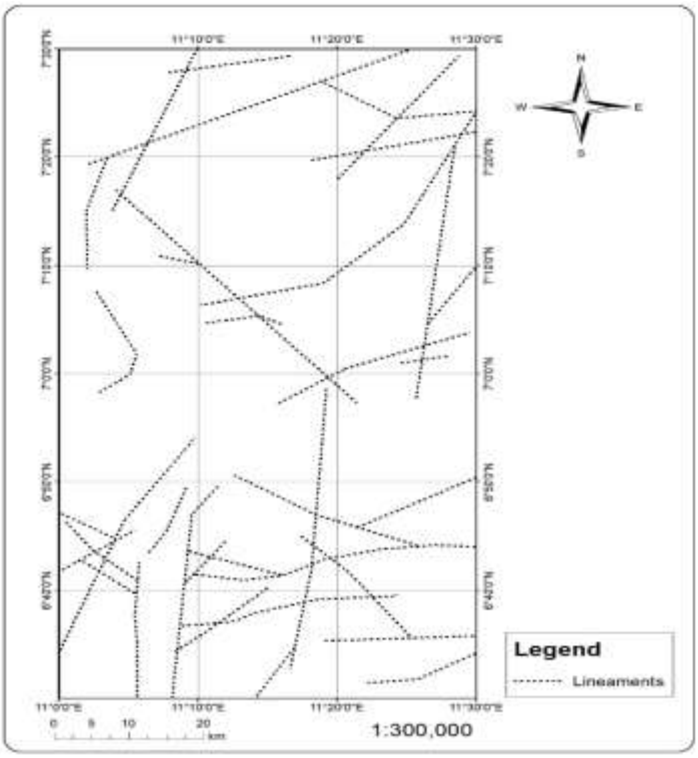

Figure 8: Structural lineaments map of the study area extracted from satellite data

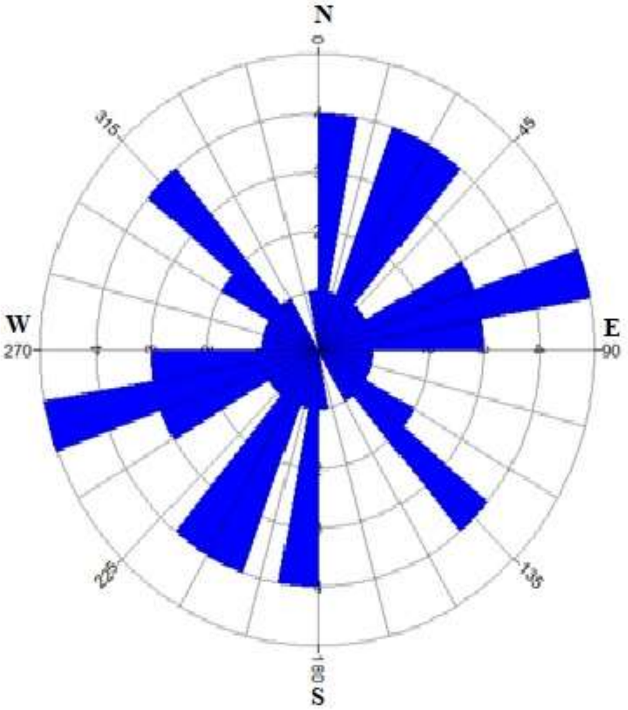

Figure 8: Rose diagram extracted from Satellite imagery, showing the main trend

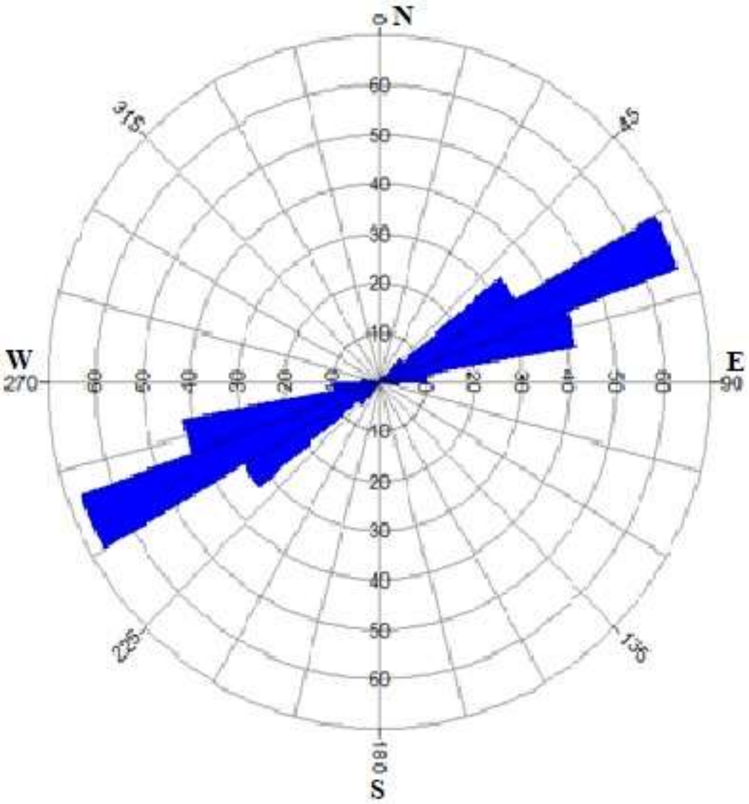

Figure 9: Rose diagram showing the structural trends from field measurement

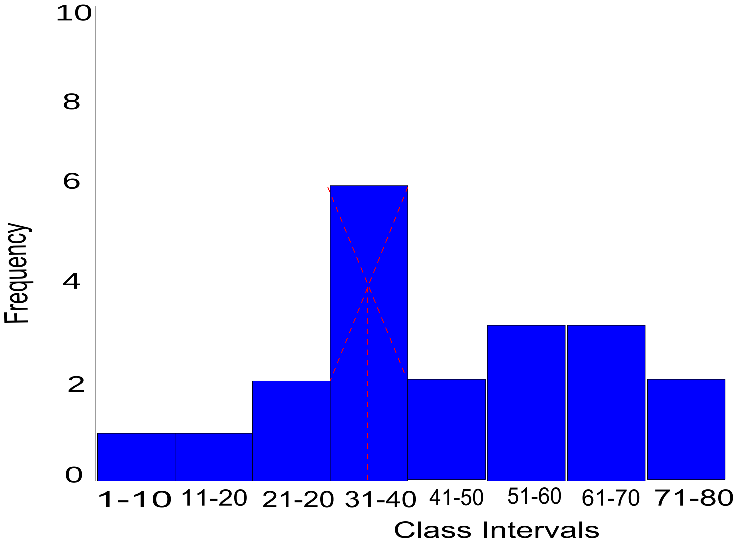

Figure 10: Histogram plot for dips angle in the area of study.

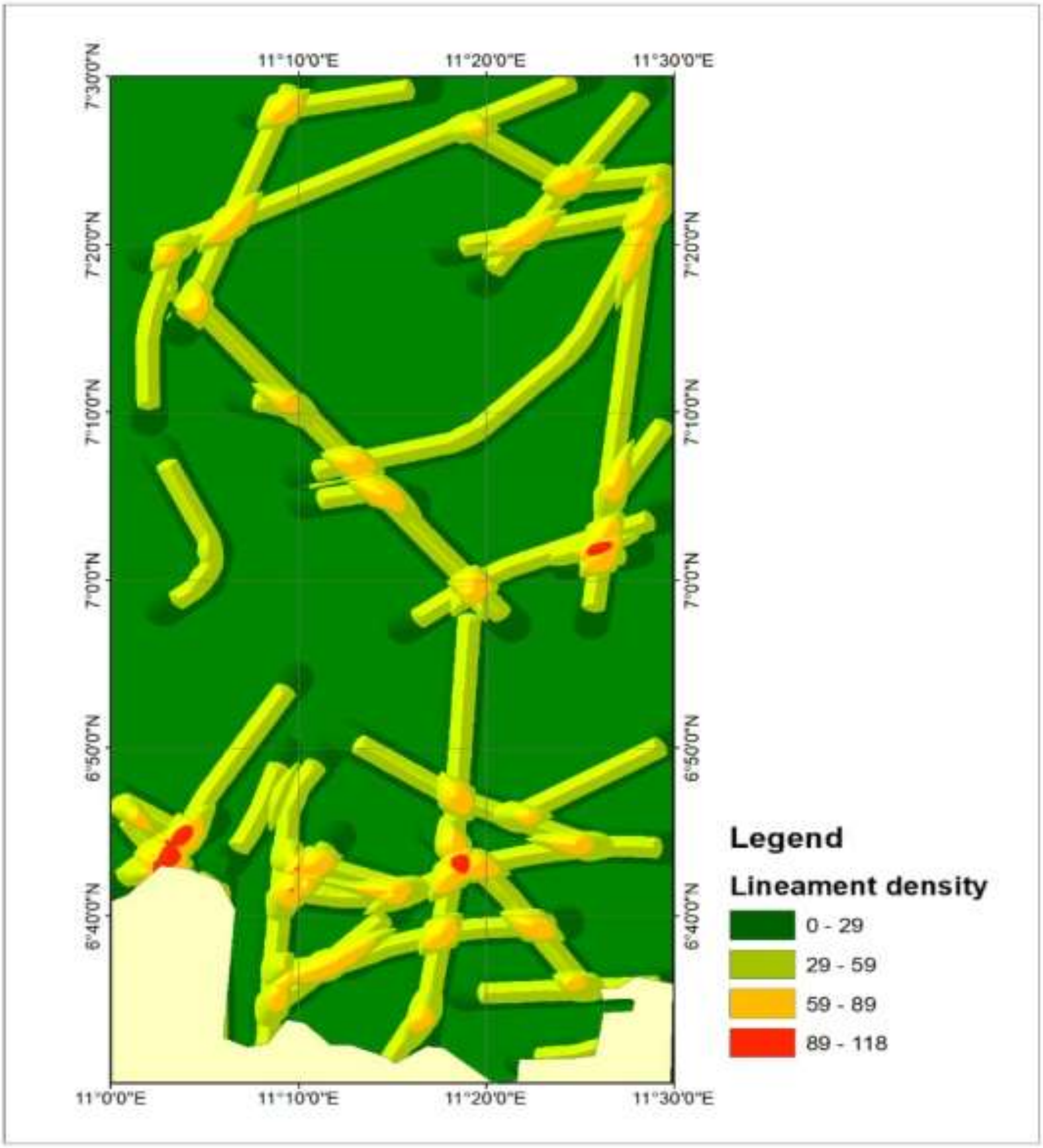

Figure 11: Lineament density map of the study area

Geochemical Characterization of veins in the study area

Ten representative samples of the analysed rocks were subjected to chemical analyses in order to ascertain the major, base metals, and base metals ratios. The analytical data for main oxides,base metals and anticipated trace element ratios are shown in Tables 6, 7, and 8. The analysed samples' average SiO_2 and Al_2O_3 contents range from 37.20 to 73.65% and 13.19 to 9.57%, respectively, according to analysis. Additionally, Fe_2O_3 percentage ranges from 9.4% to 2.3%, whereas TiO_2 content ranges from (5.13% to 0.11%). They have low concentrations of MnO and P_2O_5, which range from (0.02% to 0.07%) and (0.06% to 0.01%), whereas L_2O varies from (3.85% to 0.01%), CaO ranges from (16.64% to 2.72%), MgO ranges from (0.02% - 3.38%), Na_2O ranges from (15.91% to 1.85%), and K_2O ranges from (14.21% to 2.99%. The outcomes of SiO_2 and Al_2O_3 were found to be the most prevalent major oxides in the rocks according to the geochemical investigation for the major oxides. Because of their mode of occurrence, other oxides like CaO, Fe_2O_3, K_2O, MgO, MnO, Na_2O, P_2O_5, and TiO_2 are present in the rocks in minute to trace amounts. Whereas Al_2O_3 suggested the presence of aluminosilicate-bearing minerals like feldspar, micas, and feldspathoids, SiO2 indicated that the rocks are siliceous (Parker 1967, Fortescue, 1992, Friedrich et al., 1992). Rocks typically range from felsic to intermediate in SiO_2 content, between 37.20% and 73.65%. With compositional ranges of 13.19% - 9.65% and 10.12% - 2.33%, respectively, there are notable enrichments in Al_2O_3 and Fe_2O_3, respectively. In all the samples, their distribution patterns are fairly stable.

According to the rock geochemical analysis for base metals, nickel content ranges from 23.2 to 5.75 ppm with a mean value of 19.87 ppm, copper content ranges from 36.5 to 110 ppm with a mean value of 59.93 ppm, zinc content ranges from 13.30 to 245 ppm with a mean value of 61.84 ppm, gallium content ranges from 20.00 to 59.6 ppm with a mean value of 2.18 ppm, and germanium content ranges from 1.40 to 3.59 ppm with a mean value of 2.18 ppm.Arsenic content ranges from 3.57 to 18.10 ppm with a mean value of 10.77 ppm; Rubidium content ranges from 156 to 2090 ppm with a mean value of 550.45 ppm; Strontium content ranges from 23.6 to 961 ppm with a mean value of 333.62 ppm; Zircon content ranges from 13.90 ppm to 13.90 ppm. Silver content ranges from 7.51 to 10.3 ppm with a mean value of 8.87 ppm;

Yttrium content ranges from 6.10 to 77.9 ppm with a mean value of 21.64 ppm; Niobium content ranges from 3.33 to 24.7 ppm with a mean value of 18.67 ppm; and Barium content ranges from 26.2 to 832 ppm with a mean value of 298.27 ppm. Molybdenum content was detected in only one sample with a concentration of 3.2 ppm, and the contents of the other samples range from 7.51 to 10.3 ppm for silver, 4.75 to 17.41 ppm for tin, 18.3 to 48.7 ppm for cesium, and 9.20 to 126 ppm for lead, with a mean value of 56.90 ppm. There is only one sample with a concentration of 3.2 ppm for concentration.The concept of a geochemical background is crucial to mineral exploration. Background is described as "the normal crustal abundance of material naturally" or "the normal abundance of an element in barren earth material." The normal crustal abundance values for Au 0.0035 ppm, Sn 2.1 ppm, As 1.8 ppm, Cs 2.6 ppm, Mo 1.2 ppm, Y 31.0 ppm, V 13.60 ppm, Zr 162.0 ppm, Sr 384.0 ppm, Ba 390.0 ppm, Nb 20.0 ppm, Rb 78.3 ppm, Ni 99.0 ppm, Co 29 ppm, Cu 68 ppm, Pb 13 ppm, Ag 0.075 ppm, and Zn 76 ppm (Fortescue, 1992; Parker, 1967) A geochemical anomaly is a value that differs from the background crustal abundance and can be either positive or negative. In order to detect, characterise, and determine relative abundances of indicators, for instance, they must be present in a small number of rocks that are relatively resistant to weathering so that a reasonable dispersal train can form in rocks, sediments, or soil, be sufficiently abundant, and be visually distinct or amenable to concentrating. These minerals can reveal the type of bedrock geology (Friedrich *et al.*, 1992).

Tin (Sn), arsenic (As), cesium (Cs), molebdenum (Mo), zircon (Zr), rubidium (Rb), nickel (Ni), lead (Pb), and silver (Ag) are the rare earth elements that, according to the results, have levels greater than their crustal abundance. While MO, Ge, Cu, Sr, Nb, Ba, Y, Au, Ga, and Zn have values below their crustal abundance, their anomaly is negative because their geochemical values do not match the background crustal abundance. Because the mineralized samples had higher values for tin (Sn), arsenic (As), ceasium (Cs), molebdenum (Mo), zircon (Zr), rubidium (Rb), nickel (Ni), lead (Pb), and silver (Ag), geochemical data studies show that the area has significant mineral resources (Steiner, 2019).

Table 6: Major element composition of veins along transition zone of Mambilla and environs

Sample ID	1(%)	2(%)	3(%)	4(%)	5(%)	6(%)	7(%)	8(%)
SiO_2	38.89	70.16	71.24	47.2	62	46.12	65.11	75.35
Al_20_3	9.65	11.52	10.07	9.57	11.52	10.57	11.07	10.77
TiO_2	0.11	0.12	0.22	0.23	0.12	0.11	0.14	0.12
Fe_20_3	4.21	1.22	2.34	5.78	2.56	8.78	10.12	4.24
MnO	0.02	0.03	0.02	0.02	0.03	0.02	0.02	0.04
MgO	0.02	1.98	0.37	0.32	3.33	0.34	0.53	1.34
CaO	16.64	5.71	5.92	12.71	2.72	5.73	7.75	2.77
K_2O	11.52	6.72	6.63	13.76	12.68	14.21	3.77	2.90
Na_2O	15.91	3.81	3.88	5.86	4.87	3.85	3.88	2.90
P_2O_5	0.03	0.04	0.01	0.03	0.05	0.05	0.06	0.02
Li_2O	3.50	0.02	0.00	3.45	0.12	3.13	0.00	0.00
Total	**99.9**	**99.70**	**99.60**	**99.60**	**99.87**	**100**	**99.90**	**99.80**

Based on the base metal ratio results (Table 8), the K/Rb ratios of samples 1, 4, 6, 9, and 10 are 4.8 ppm or higher. Thus, they are pointing to bedrock that has been fractionated and may contain a lithium deposit. The lithium-bearing pegmatites are called lithium-cesium-tantalum pegmatites because of their enrichment in the incompatible elements Li, Cs, Sn, Rb, and Ta (Steiner, 2019). The result is consistent with the geochemistry of major oxides, base metal composition ratio, and concentration. Samples related to mineralization were found in Samples 1, 4, 6, 9, and 10 (Table 8) (Meima et al., 197; Kampang (2010); Plimer and Elliott, 2019). According to Filzmoser et al. (2005), the rocks are of crustal origin and typically have silica contents of more than 60%.

Table 7: Base metals composition of veins along transition zone of Mambilla and environs

Sample ID	Ni (ppm)	Cu (ppm)	Zn (ppm)	Ga (ppm)	Ge (ppm)	As (ppm)	Rb (ppm)	Sr (ppm)	Zr (ppm)	Y (ppm)	Nb (ppm)	Mo (ppm)	Ag (ppm)	Sn (ppm)	Cs (ppm)	Ba (ppm)
1	13.7	39.2	59.1	38.2	1.93	8.71	694	24.6	32.4	21.2	24.5	1.3	8.29	14.4	ND	41.8
2	9.34	38.4	29.8	38.6	1.4	18.1	288	23.3	84.1	23.9	15.5	ND	8.58	12.2	ND	41.2
3	21.8	110	43.3	20.1	ND	ND	167	642	84.9	32.2	3.33	1.9	8.71	ND	ND	574
4	87.5	67.7	247	40.1	ND	16.5	520	781	434	77.9	17	ND	9.61	5.69	18.3	399
5	12.6	46.3	33	47.3	ND	ND	156	466	121	12.7	ND	4.1	8.11	ND	ND	140
6	13.3	33.6	30.1	59.5	3.3	ND	590	23.1	46.3	11.4	43.4	ND	ND	66.3	ND	31.1
7	5.75	36.5	13.3	30.7	ND	10.5	616	66.5	50.4	14.7	4.3	3.2	7.47	12.5	ND	178
8	24.5	79	189	45.3	ND	ND	358	961	358	23.9	8.35	ND	10.5	4.75	ND	832
9	23.2	68.2	150	41.1	ND	ND	305	900	349	27.7	11.8	ND	7.51	ND	ND	738
10	15.4	46.6	23.9	40.8	2.14	11.1	196	35.8	84.8	18.6	17.3	3.1	ND	17.4	ND	52.8
Crustal abundance (Fortescue, 1992)	99	68	76	10.5	1.2	1.8	78.3	384	162	31	20	1.2	0.75	2.1	2.6	390

Table 8: Base metals ratios used as finger prints in understanding the origin, mineralization and evolution of rocks in the study area

Sample ID	Rb/Nb (ppm)	K/Rb (ppm)	Sr/Cu (ppm)	Rb/Zr (ppm)	Y+Nb (ppm)	Rb/Sr (ppm)
1	154.22	8.20	0.62	21.42	45.7	28.21
2	18.58	1.62	0.60	3.42	39.40	0.67
3	50.15	2.74	5.83	1.97	35.53	0.26
4	30.59	10.63	11.53	12.06	94.90	12.38
5	156	2.81	10.06	1.29	12.70	0.33
6	13.72	7.10	0.08	12.83	54.80	25.54
7	143.26	3.87	10.40	20.28	19.00	9.26
8	42.87	2.41	12.16	1.02	32.25	0.37
9	25.85	9.78	13.20	0.87	39.50	0.34
10	11.33	4.10	0.77	2.31	35.90	5.47

CONCLUSION

This work discusses how to characterise the hydrothermal alteration zone across the Mambilla Plateau and its surroundings by combining remote sensing datasets, field measurement, and geochemical data. The primary goal of the planned Landsat 8 and ASTER studies was to classify the different types of hydrothermal alteration and structural lineaments in the area. Band ratios 6/7 and 6/5 were used to show changes in clay, 6/5 and 4/2 to identify zones of change in ferrous ion, and 4/2 and 4/2 to highlight variations in ferric ion, in accordance with Landsat 8 imagery. However, for ASTER mapping of hydrothermal alteration, band ratios of 4/6, 5/6, 5/8, 2/1, and (5/3+1/2) were employed. Four distinct band ratio changes were observed: argillic on band ratio 4/6, phyllic on band ratio 5/6, propylitic on band ratio 5/8, and ferric iron on band ratio 2/1. The band ratio (5/3+1/2) was used to show the variation in ferrous ion alteration by region. A rose diagram analysis was used to identify the main structure directions, with N-S, NE-SW, and NNE-SSW being the most noticeable. Significant tectonic changes have occurred in the studied area, especially those related to the Pan-African orogeny. These led to the nearby formation of multiple joints, faults, and fractures. The basement rocks in the area are mostly made up of younger volcanic basalts, migmatite gneiss, and granite gneiss. Field geological research has revealed three types of alteration: phyllic, argillic, and propylitic. Numerous notable alteration processes, such as epidotization, sericitization, muscovitization, kaolinitization, and chloritization, have been identified as a result of the area's significant deformation following regional metamorphism.. Geochemically, on average, the Al_2O_3, SiO_2, Fe_2O_3, CaO, MgO, K_2O, Na_2O, Li_2O content are 12.04%; 54.83%; 4.76%, 7.16 %, 3.02 %, 10.22%, 4.53%, 1.35% correspondently while MnO, P_2O_5 and TiO_2 are less than 1%. suggesting an oxide facies type for the deposit. The average base metal composition ranges from Ni (19.87 ppm), Cu (59.93 ppm), Zn (61.84 ppm), Ga (37.30 ppm), Nb (18.67 ppm), Ge (2.18 ppm), As (10.77 ppm), Rb (550.45 ppm), Sr (333.62 ppm), Y (21.64 ppm), Ba (298.27 ppm), Mo (3.2 ppm), Ag (8.87 ppm), Sn (14.0 ppm), and Zr (134.55 ppm). Base metals such as tin (Sn), arsenic (As), ceasium (Cs), molebdenum (Mo), zircon (Zr), rubidium (Rb), nickel (Ni), lead (Pb), and silver (Ag) have have positive anomaly because their values are higher than the background crustal abundance, while Mo, Ge, Cu, Sr, Nb, Ba, Y, Au, Ga, and Zn have values below their crustal abundance; their anomaly is negative. From their ratios, samples 1, 4, 6, 9, and 10 showed high Sr/Cu, Rb/Zr, Y+Nb, Rb/Nb, and K/Rb ratios of 4.8 ppm and above. They are indicating high potential for host mineralization. Tectonically, the major trends in the area are NE-SW, NNE-SSW, and N-S. Lithium, titanium, and silica oxides were present in significant amounts, based on the geochemical analysis of the samples. The mineralization in the area is structurally controlled.

CONFLICT OF INTEREST

The authors declare that the research was conducted in the absence of any commercial or financial relationships that could be construed as a potential conflict of interest.

REFERENCES

Abdul Malik, N.F.; Garba, I.; Danbatta, U.A.; Hamza, H (2018). Delineation and correlation of lineaments using landsat-7 ETM+, DEM and aeromagnetic datasets: Basement complex of shanono, northwestern Nigeria. J. Geol. Geophys, 7, 445.

Abdi, H. and Williams, L.J.(2010). Principal component analysis.*Wiley Interdisciplinary Reviews: Computational Statistics*, vol. 2. pp. 433–459.

Abhary, A. and Hassani, H. 2016. Mapping hydrothermal mineral deposits using PCA and BR methods in Baft 1: 100000 Geological Sheet, Iran. 2. http://www .academia .edu/ 28268172/ Mapping_HydrothermalMineral_De posits UsingPCA and BR Methods in Baft1100000 Geological Sheet_Iran

Abrams, M.; Crippen, R.; Fujisada, H (2020).ASTER global digital elevation model (GDEM) and ASTER global water body dataset (ASTWBD).Remote Sens., 12, 1156.

Ananaba, S.E.; Ajakaiye, D.E(1987). Evidence of tectonic control of mineralization in Nigeria from lineament density analysis A Landsat-study.Int. J. Remote Sens. 8, 1445–1453.

Antoine, D (2013). TravauxPratiques de télédétectionspatiale.Arlon Campus Environnement, Université de Liège, Belgique, 84p.

Bedini, E. 2009.Mapping lithology of the Sarfartoqcarbonatite complex, southern West Greenland, using HyMap imaging spectrometer data.*Remote Sensing of Environment*, vol. 113.pp.1208–1219.

Bemis, S.P., Micklethwaite, S., Turner, D., James, M.R., Akciz, S., Thiele, S.T.,andBangash, H.A. (2014). Ground-based and UAV-based photogrammetry: A multi-scale, high-resolution mapping tool for structural geology and paleoseismology. *Journal of Structural Geology*, vol. 69, no. 1. pp. 63–178.

Berk, A., Bernstein, L., Anderson, G., Acharya, P., Robertson, D., Chetwynd, J., and Adler-Golden, S. (1998). Modtrancloud and multiple scattering upgrades with application to AVIRIS. *Remote Sensing of Environment*,vol. 65. pp. 367–375.

Bhattacharya, S., Majumdar, T., Rajawat, A., Panigrahi, M., and Das, P. (2012).Utilization of Hyperion data over Dongargarh, India, for mapping altered/weathered and clay minerals along with field spectral measurements.*International Journal of Remote Sensing*, vol. 33. pp. 5438–5450.

Black R (1980). Precambrian of West Africa. Episodes 4:3–8

Boardman, J. W. and Kruse, F. A(1994). Automated spectral analysis: a geological example using AVIRIS data, north Grapevine Mountains, Nevada: in Proceedings, ERIM Tenth Thematic Conference on Geologic Remote Sensing. Environmental Research Institute of Michigan, Ann Arbor, MI, pp. I-407-418.

Burke K.C, and Dewey J.F (1972). Orogeny in Africa. In: Dessauvagie TFJ, Whiteman AJ (eds), Africageology. University of Ibadan Press, Ibadan, pp 583–608

Calvin, W.M., Littlefield, E.F., and Kratt, C. (2015).Remote sensing of geothermal-related minerals for resource exploration in Nevada.*Geothermics*, vol. 53.pp. 517--526.

Chander, G. and Markham, B. (2003).Revised Landsat-5 TM radiometric calibration procedures and postcalibration dynamic ranges.*IEEETransactions on Geoscience and Remote Sensing*, vol. 41. pp. 2674–2677.

Chavez, P.S. (1996).Image-based atmospheric corrections-revisited and improved.*Photogrammetric Engineering and Remote Sensing*, vol. 62. pp. 1025–1035.

Cheng, Q., Bonham-Carter, G., Wang, W., Zhang, S., Li, W., and Qinglin, X. (2011) .A spatially weighted principal component analysis for multi-element geochemical data for mapping locations of felsic intrusions in the Gejiu mineral district of Yunnan, China.*Computers & Geosciences*, vol. 37.pp. 662–669.

Ciampalini, A., Garfagnoli, F., Antonielli, B., Moretti, S., and Righini, G. (2013). Remote sensing techniques using Landsat ETM+ applied to the detection of iron ore deposits in Western Africa. *Arabian Journal of Geosciences*, vol. 6. pp. 4529–4546.

Clark, R.N., King, T.V., Klejwa, M., Swayze, G.A., and Vergo, N. (1990).High spectral resolution reflectance spectroscopy of minerals.*Journal ofGeophysical Research: Solid Earth*, vol. 95. pp. 12653–12680.

Clark, R.N. (1999). Spectroscopy of rocks and minerals, and principles of spectroscopy.*Manual of Remote Sensing*, vol. 3. pp. 2.2–2.4.

Dada .S.S (2006). Proterozoic evolution of Nigeria. In: Oshi O (ed) The basement complex of Nigeriaand its mineral resources (A Tribute to Prof. M. A. O. Rahaman). Akin Jinad& Co. Ibadan,pp 29–4

Da Cunha Frutuoso, R.M. (2015).Mapping hydrothermal gold mineralization using Landsat 8 data.A case of study in Chaves license, Portugal.https://sigarra.up.pt/fcup/pt/pub_geral.show_file?pi_doc_id=44053

Deslandes, S (1989). Initiation aux méthodes de traitementnumérique des images satellites, sur le système PCI Inc. EASUPACE. CARTEL. 32p

Di Tommaso, I. and Rubinstein, N. (2007). Hydrothermal alteration mapping using ASTER data in the Infiernillo porphyry deposit, Argentina. *Ore GeologyReviews*, vol. 32. pp. 275–290.

Dos Santos, M.A.; van Lier, Q.D.; van Dam, J.C.; Freire, A.H(2016). Determination of empirical parameters for root water uptake models.Hydrol. Earth Syst. Sci. Discuss, 21, 473–493.

Drews-Armitage, S., Romberger, S., and Whitney, C. (1996). Clay alteration andGold deposition in the Genesis and Blue Star deposits, Eureka County, Nevada. *Economic Geology*, vol. 91. pp. 1383–1393.

Dupreez.J.W, Barber W (1965).The distribution and chemical quality of ground water in Northern Nigeria.Bulletin 36.Geological survey of Nigeria 93.

El-Makky, A.M. (2011). Statistical analyses of La, Ce, Nd, Y, Nb, Ti, P, and Zr inbedrocks and their significance in geochemical exploration at the UGarayat gold mine Area, Eastern Desert, Egypt. *Natural ResourcesResearch*, vol. 20.pp. 157.

Filzmoser P, Garrett RG, and Reimann C (2005) Multivariate outlier detection in exploration geochemistry. Computers and Geosciences 31: 579–587.

Frantz C (1981). Development without communities: Social fields, Network and Action in the Mambilla Grasslands of Nigeria. J. Human org. pp. 211-220.

Fortescue, J.A.C(1992). Regional Geochemical Mapping.Geophysics/Geochemistry Section, Ontario Geological Survey, PP1348-1394.

Gabr, S., Ghulam, A., and Kusky, T. (2010). Detecting areas of high-potentialgold mineralization using ASTER data. *Ore Geology Reviews*, vol. 38.pp. 59–69.

Gale.E.(2017).Education, learning and research resources.https://www.gale.com/Accessed 15 November 2017.

Gholami, R., Moradzadeh, A., and Yousefi, M. (2012).Assessing the performance of independent component analysis in remote sensing data processing.*Journal of the Indian Society of Remote Sensing*, vol. 40. pp. 577–588.

Grunsky, E.C., Mueller, U.A., and Corrigan, D. (2014). A study of the lake sediment geochemistry of the Melville Peninsula using multivariatemethods: applications for predictive geological mapping. *Journal ofGeochemical Exploration*, vol. 141. pp. 15–41.

Han, T. and Nelson, J. (2015). Mapping hydrothermally altered rocks withLandsat 8 imagery: A case study in the KSM and Snowfield zones,northwestern British Columbia. British Columbia Geological Survey.

Horel, J. (1984). Complex principal component analysis: Theory and examples.*Journal of Climate and Applied Meteorology*, vol. 23. pp. 1660–1673.

Holmes, R. and Lu, L. (2015). Introduction: Overview of the global iron oreindustry. *Iron Ore*. Elsevier.

Hung, L.Q.; Batelaan, O.; De Smedt, F(2005).Lineament extraction and analysis, comparison of LANDSAT ETM and ASTER imagery. Case study: Suoimuoi tropical karst catchment, Vietnam. In Proceedings of the Remote Sensing for Environmental Monitoring, GIS Applications, and Geology V, Bruges, Belgium, 19–22 September; Volume 5983, pp. 182–193.

Ibrahim, I.H (2013). Impact of Structural Lineaments on Mineralized Occurrences in North Abu Rusheid-Sikait Area, South Eastern Desert, Egypt. In Proceedings of the 5th Tunisian Days of Applied Geology JTGA 2013, Hammamet, Tunisia, 17–20 May; pp. 227–251.

Immaculate, N.-F.M.; Tende, A.W.; Fouateu, Y.R.; Marc, A.F.Q(2020). Remote sensing for geological investigation of Mayo Kila and environs, north west region of Cameroon. Am. J. Earth Sci, 7, 1–12.

Jeje L.K (1983). Aspects of geomorphology of Nigeria.Heinemann educational books.

Johnson, J.R., Bell III, J.F., Bender, S., Blaney, D., Cloutis, E., Ehlmann, B.,Fraeman, A., Gasnault, O., Kinch, K., and Le Mouelic, S. (2016). Constraintson iron sulfate and iron oxide mineralogy from ChemCam visible/nearinfraredreflectance spectroscopy of Mt. Sharp basal units, Gale Crater,Mars. *American Mineralogist*, vol. 101. pp. 1501–1514.

Jolliffe, I.T. (2002). Principal component analysis and factor analysis.*PrincipalComponent Analysis*. Springer. pp. 150–166.

Kamgang, P, Njonfang, E, Nono, A, Dedzo M. G. &Tchuoa, F. M.(2010). Petrogenesis of silicic magma system: Geochemical evidence from Bamenda Mountains, NW Cameroon, Cameroon Volcanic Line", J. Afr. Earth Sci. 58 285.https://doi.org/10.1016/j.jafrearsci.2010.03.008

Kaiser, P.K., Henning, J.G., Cotesta, L., and Dasys, A. (2002).Innovations in mine planning and design utilizing collaborative immersive virtual reality (CIRV).*Proceedings of the 104th CIM Annual General Meeting*. CIM, Montreal.

Kotnise, G. and Chennabasappa, S. (2015). Application of remote sensing techniques in identification of lithological rock units in southern extensionof Kolar Schist Belt from Chigargunta, Chittoor District, Andhra Pradesh toMaharajagadai, Krishnagiri District, Tamil Nadu.*International Journal ofInnovative Science, Engineering Technology*, vol. 2, no. 11.

Kruse, F.A., Lefkoff, A.B., Boardman, J.W., Heidebrecht, K.B., Shapiro, P.J. and Goetz, A.F.H. (1993) The Spectral Image Processing System (SIPS)-Interactive Visualization and Analysis of Imaging Spectrometer Data. Remote Sensing of Environment, vol. 44, p. 145-163.

Kruse, F. A., Lefkoff, A. B., Boardman, J. W.,(1993). The spectral image processing system (SIPS)-interactive visualization and analysis of imaging spectrometer data. In: AIP Conference Proceedings. American Institute of Physics, p. 192-201.

Linnen, R.L., Van Lichtervelde, M.., &ˇCerný, P. (2012). Granitic pegmatites: Granitic pegmatites as sources of strategic metals. Elements 2012, 8, 275–280.

Loughlin, W. (1991).Principal component analysis for alteration mapping.*Photogrammetric Engineering and Remote Sensing*, vol. 57.pp. 1163–1169.

Maduaka, A.C. (2014). Contributions of solid mineral sectors to Nigeria's economic development.Eastern Mediterranean University (EMU) and DoğuAkdenizUniversitesi (DAU).

Mahandani, S., Puta, I., Hirawan, A., Abbas, R., and Titisari, A. (2018).Integrated remote sensing and geological mapping to identify landslideprone zone in Loano, Purworejo, Central Java. *Proceedings of EAGE-HAGI1st Asia Pacific Meeting on Near Surface Geoscience and Engineering*.doi:10.3997/2214-4609.201800372

Mahboob, M.A., Atif, I., and Iqbal, J. (2015).Remote sensing and GIS applications for assessment of urban sprawl in Karachi, Pakistan.*Science,Technology and Development*, vol. 34. pp. 179–188.

Mahboob, M.A., Iqbal, J., and Atif, I. (2015). Modeling and simulation of glacier avalanche: A case study of gayari sector glaciers hazards assessment. *IEEE Transactions on Geoscience and Remote Sensin*g, vol. 53. pp. 5824–5834.

Manley, M. (2014). Near-infrared spectroscopy and hyperspectral imaging: nondestructive analysis of biological materials. *Chemical Society Reviews*,vol. 43. pp. 8200–8214.

Marjoribanks, R. (2010). Geological mapping in exploration.*Geological Methods in Mineral Exploration and Mining*.Springer.

Mould .A.W. S (1960). Report on a rapid reconnaissance soil survey of the Mambilla plateau. Bulletin 15, Soil survey section, regional research station, ministry of agriculture, Samaru, Zaria.

Masek, J.G., Vermote, E.F., Saleous, N.E., Wolfe, R., Hall, F.G., Huemmrich,K.F., Gao, F., Kutler, J., and Lim, T.-K. (2006). A Landsat surfacereflectance dataset for North America, 1990-2000. *IEEE Geoscience andRemote Sensing Letters*, vol. 3. pp. 68–72.

Meima, J.A.; Rammlmair, D.; Junge, M.(**2022**) .The use of Laser Induced Breakdown Spectroscopy for the mineral chemistry of chromite, orthopyroxene and plagioclase from Merensky Reef and UG-2 chromitite, Bushveld Complex, South Africa. Chem. Geol., 589, 120686

Mia, B. and Fujimitsu, Y. (2012).Mapping hydrothermal altered mineral depositsusing Landsat 7 ETM+ image in and around Kuju volcano, Kyushu, Japan.*Journal of Earth System Science*, vol. 121. pp. 1049–1057.

Mubi AM, Tukur. A.L (2005).Geology and relief of Nigeria. Nigeria. Heinemann educational books.

Novak, I. and Soulakellis, N. (2000).Identifying geomorphic features usingLANDSAT-5/TM data processing techniques on Lesvos, Greece.*Geomorphology*, vol. 34. pp. 101–109.

Obaje N.G. (2009). The Basement Complex. In: Geology and Mineral Resources of Nigeria. Lecture Notes in Earth Sciences, vol 120. Springer, Berlin, Heidelberg.

Parker C.A(1967). Fluorescence and Phosphorescence Analysis, Admiralty materials laboratory, holtonhearn, poole, dorsetvol 4 issue5.

Plaza, A. and Chang, C. (2005) Fast implementation of pixel purity index algorithm. Algorithms and Technologies for Multispectral, Hyperspectral, and Ultraspectral Imagery XI, 28 March 2005, Orlando, FL, USA, vol. 5806, p. 307-317.

Plimer, I.R.; Elliott, S.M. (1979).The use of Rb/Sr ratios as a guide to mineralization. J. Geochem. Explor., 12, 21–34.

Friedrich, G, Marker, A, and Kanig , M (1992) Heavy mineral surveys in exploration of lateritic terrain. In: Butt CRM and Zeegers H (eds.) Handbook of Exploration Geochemistry, Vol. 4: Regolith Exploration Geochemistry in Tropical and Subtropical Terrains, pp. 483–498. Amsterdam: Elsevier.

Pour, A.B. and Hashim, M. (2012). The application of ASTER remote sensingdata to porphyry copper and epithermal gold deposits.*Ore GeologyReviews*, vol. 44. pp. 1–9.

Pour, A.B. and Hashim, M. (2015). Regional hydrothermal alteration mapping using Landsat-8 data.*Proceedings of Space Science and Communication(IconSpace)* 2015.IEEE. pp. 199–202.

Pournamdari, M., Hashim, M. and Pour, A.B. (2014).Spectral transformation ofASTER and Landsat TM bands for lithological mapping of Soghanophiolite complex, south Iran.*Advances in Space Research,* vol. 54, no. 4.pp. 694–709.

Ramakrishnan, D. and Bharti, R. (2015).Hyperspectral remote sensing and geological applications.*Current Science*, vol. 108. pp. 879–891.

Repacholi, M. (2012). Clay Mineralogy: Spectroscopic and Chemical Determinative Methods. Springer Science & Business Media.

Richter, R. (1997). Correction of atmospheric and topographic effects for highspatial resolution satellite imagery.*International Journal of RemoteSensing*, vol. 18. pp. 1099–1111.

Richards, J. A.(1999). Remote sensing digital image analysis. Berlin et al.: Springer.

Roy, D.P., Kovalskyy, V., Zhang, H., Vermote, E.F., Yan, L., Kumar, S., andEgorov, A. (2016).Characterization of Landsat-7 to Landsat-8 reflectivewavelength and normalized difference vegetation index continuity.*Remote Sensing of Environment*, vol. 185. pp. 57–70.

Safari, M., Maghsoudi, A., and Pour, A.B. (2017). Application of Landsat-8 andASTER satellite remote sensing data for porphyry copper exploration: acase study from Shahr-e-Babak, Kerman, south of Iran. *GeocartoInternational*, May 2017. pp. 1–16.

Sadiq, S.; Muhammad, U.; Fuchs, M (2022). Investigation of landslides with natural lineaments derived from integrated manual and automatic techniques applied on geospatial data. Nat. Hazards, 110, 2141–2162.

Sabins, F.F. (2007). *Remote Sensing: Principles and Applications*, Waveland Press.

Sabins, F. F. (1999). Remote sensing for mineral exploration.*Ore Geology Review*s, vol. 14. pp. 157–183.

Schroeder, T. A., Cohen, W.B., Song, C., Canty, M.J., and Yang, Z. (2006).Radiometric correction of multi-temporal Landsat data for characterizationof early successional forest patterns in western Oregon. *Remote Sensing ofEnvironment*, vol. 103. pp. 16–26.

Schwertmann, U. (1993). Relations between iron oxides, soil color, and soilformation. *Soil Color*.Bigham, J.M. and Ciolkosz, E.J. (eds.). *Soil ScienceSociety of America*. pp. 51–69.

Short, N.M. And lowmanjr, P.D. (1973). Earth observations from space: Outlook for the geological sciences. Goddard space flight center, Greenbelt, md.

Song, C., Woodcock, C.E., Seto, K. C., Lenney, M.P., and Macomber, S.A. (2001).Classification and change detection using Landsat TM data: When andhow to correct atmospheric effects? *Remote Sensing of Environment,*vol. 75. pp. 230–244.

Song, C. and Woodcock, C.E. (2003).Monitoring forest succession withmultitemporal Landsat images: Factors of uncertainty.*IEEE Transactionson Geoscience and Remote Sensing*, vol. 41. pp. 2557–2567.

Steiner, B.M.(2019). Tools and Workflows for Grassroots Li–Cs–Ta (LCT) Pegmatite Exploration.Minerals, 9, 499.

Tangestani, M. and Moore, F. (2001). Comparison of three principal componentanalysis techniques to porphyry copper alteration mapping: a case study,Meiduk area, Kerman, Iran. *Canadian Journal of Remote Sensing*, vol. 27.pp. 176–182.55.

Tedesco, S.A. (2012). Surface Geochemistry in Petroleum Exploration.Springer Science & Business Media.

Tripp, G.I.; Vearncombe, J.R(2004). Fault/fracture density and mineralization: A contouring method for targeting in gold exploration. J. Struct. Geol. , 26, 1087–1108.

Tukur, A. L, Adebayo. A. A, Galtima A (2005). The land and people of the Mambilla Plateau, Nigeria. Heinemann educational .

Udvardi, B., Kovacs, I.J., Fancsik, T., Konya, P., Batori, M., Stercel, F., Falus,G., and Szalai, Z. (2017).Effects of particle size on the attenuated totalreflection spectrum of minerals.*Applied Spectroscopy*, vol. 71.pp. 1157–1168.

Van Der Meer, F. (2004). Analysis of spectral absorption features inhyperspectral imagery. *International Journal of*

Applied Earth ObservationandGeoinformation, vol. 5. pp. 55–68.

Vermote, E., Justice, C., Claverie, M., and Franch, B. (2016).Preliminary analysisof the performance of the Landsat 8/OLI land surface reflectance product.*Remote Sensing of Environment*, vol. 185. pp. 46–56.

Vermote, E. F., Tanre, D., Deuze, J. L., Herman, M., and Morcette, J.-J.(1997).Second simulation of the satellite signal in the solar spectrum, 6S: Anoverview. *IEEE Transactions on Geoscience and Remote Sensing*, vol. 35.pp. 675–686.

Wessels, R L., Vaughan, R.G., Patrick, M.R., and Coombs, M.L. (2013).Highresolutionsatellite and airborne thermal infrared imaging of precursoryunrest and 2009 eruption at Redoubt Volcano, Alaska.*Journal ofVolcanology and Geothermal Research*, vol. 259. pp. 248–269.

Weerasekara, W.L.; Mayadunna, B.B.; Senanayake, I.P.; Dissanayake, D(2014). Integrated remote sensing and GIS in lineament mapping for groundwater exploration–A case study in Ambalantota, Sri Lanka. In Proceeding of SAITM Research Symposium on Engineering Advancements; South Asian Institute of Technology and Medicine: Malabe, Sri Lanka; p. 62e65.

Yusuf, S.N.; Kuku, A.Y.; Ibrahim, Y.; Kasidi, S (2019).Tectono-metamorphic deformation and structures of Mubi-Hong area, NE, Nigeria. Niger. J. Technol. Dev. **2**, 16, 201–212.

Zaini, N., Van Der Meer, F., Van Ruitenbeek, F., De Smeth, B., Amri, F., andLievens, C. (2016). An alternative quality control technique for mineralchemistry analysis of Portland cement-grade limestone using shortwaveinfrared spectroscopy.*Remote Sensing*, vol. 8.p. 950.

Zanter, K. (2016). Landsat 8 (L8) data users handbook.https://landsat.usgs.gov/landsat-8-l8-data-users-handbook accessed 20 January 2018.

Zhang, X., Pazner, M., and Duke, N. (2007).Lithologic and mineral information extraction for gold exploration using ASTER data in the south Chocolate Mountains (California).*ISPRS Journal of Photogrammetry and RemoteSensing*, vol. 62. pp. 271–282.

.